

EXTRACTING POWER IN JET STREAMS: PUSHING THE PERFORMANCE OF FLAPPING WING TECHNOLOGY

M.F. Platzer*, M.A. Ashraf**, J. Young**, and J.C.S. Lai**

*AeroHydro R&T Associates, Pebble Beach, CA, USA

**School of Engineering and Information Technology, University of New South Wales, Australian Defence Force Academy, Canberra, Australia

Abstract

This paper addresses the problem of power extraction from high-altitude wind streams by means of tethered wings with attached flapping-wing power generators. A new type of flapping-wing power generator is described. It is shown in experiments and Navier-Stokes computations that the square-wave type oscillations of this new generator provide a substantially increased power output and efficiency compared to previously investigated sinusoidally oscillating generators. It is concluded that the mechanical simplicity and increased performance of the new generator justify the further development of this power extraction concept.

1 Introduction

With the rapid increase in the worldwide use of energy coupled with the depletion of fossil fuel resources and the need to significantly reduce greenhouse gas emissions, the development of means to extract energy from renewable sources has seen unprecedented attention and urgency. While the surface wind power density is approximately 1.2 kW/m², the power density of the jet streams is estimated to be around 16 kW/m² [1]. Therefore it would be attractive if this energy could be harvested.

The extraction of power from an air stream is a phenomenon well known to aeronautical engineers. Consider an airfoil which is free to oscillate vertically and in pitch, as shown in Fig. 1. If the combined oscillation occurs in such a manner that there is a 90 degree phase angle ϕ between the pitch and the plunge (vertical) motion, then the aerodynamic lift is always in the same direction as the motion of the foil, as shown in Fig. 1a. In this case, work

is done by the air on the foil throughout the complete cycle. In other words, the foil is extracting energy out of the air flow. On the other hand, if the phasing between pitch and plunge is zero, as shown in Fig. 1b, then during parts of the cycle the aerodynamic lift opposes the motion and no net work is done on the foil. The type of flutter shown in Fig. 1a can easily occur on airplane wings for certain values of the bending and torsional stiffnesses of the wing. Clearly, this phenomenon can also be used for power generation.

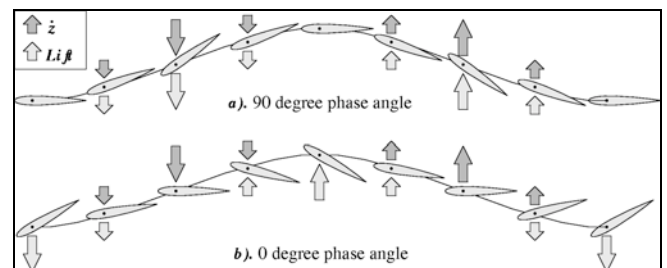


Fig. 1. Bending-Torsion Foil Flutter

By exploiting the knowledge gained in our research into flapping-wing micro-air vehicles [2-4] we proposed in ICAS 2008 [1] a novel concept of using flapping wing power generators to extract the abundant energy available in high altitude jet streams. The implementation of any flying electric generator will require minimum weight and drag while maximizing the power output and efficiency. In our previous paper [1] we proposed a tethered wing with an attached flapping-wing power generator. We argued that such a configuration may have weight and performance advantages over other configurations currently being investigated. In reference [3] we demonstrated a small-scale flapping-wing power generator

where the phase angle between the pitch and plunge motions was enforced with a mechanical control system. Although successful, this design has the disadvantage of requiring several mechanical parts which cause additional weight and potential operational and maintenance problems. To overcome this disadvantage we proposed a new generator which requires no elaborate mechanical control system. Instead the pitch-plunge phasing is induced by the flow itself.

It is the purpose of our paper to document the progress achieved in the development of this new flapping-wing power generator. To this end, the experimental progress is described in Section 2, followed by a discussion of the computational analysis in support of the experiment.

2. Development of New Power Generator with Flow-Induced Pitch-Plunge Phasing

Fig. 2 illustrates the basic principle of the new power generator. An airfoil is shown which can slide on a rail guide. Furthermore it can pitch about a pitch axis which is located downstream of the mid-chord point. This ensures that the airfoil is statically unstable so that it deflects to an increasing pitch angle until it is stopped by a mechanical restraint. In Fig. 2 the flow is assumed to be from left to right and the airfoil is therefore sliding to the left because of the lift generated by the airfoil's pitch angle.

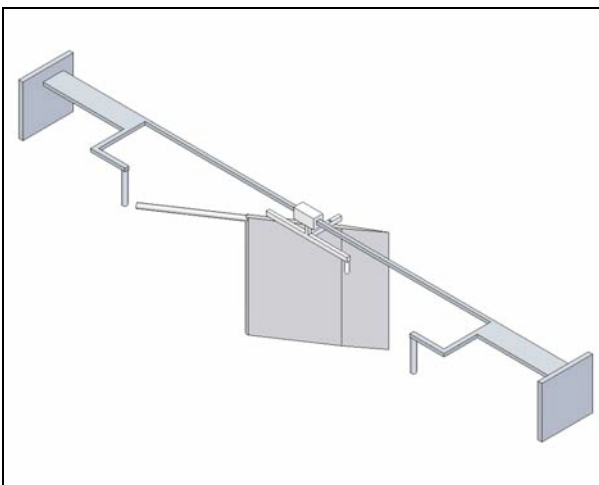


Fig. 2. Aerodynamically controlled power generator (wing in mid-stroke).

In Fig. 3 the airfoil starts to turn counterclockwise because the airfoil's "finger" started to touch the control rod shown in Fig. 2 and Fig. 3. An aerodynamic moment is generated which initiates the stroke reversal by pitching the airfoil past the zero pitch angle. As a result the airfoil is now generating a lift force in the opposite direction and the airfoil starts to slide to the right. The process repeats itself at the other end and a square-wave type oscillation is being generated. The computational analysis in Section 3 reveals that square-wave type oscillation is more effective than a pure sinusoidal oscillation enforced by a mechanical control system.

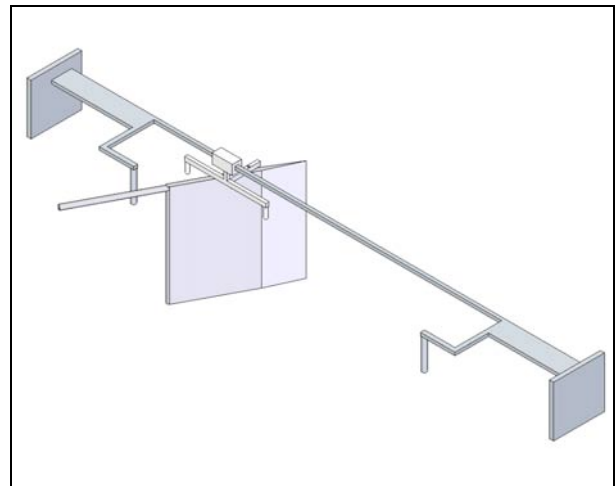


Fig. 3. Aerodynamically controlled power generator (wing at end-stroke).

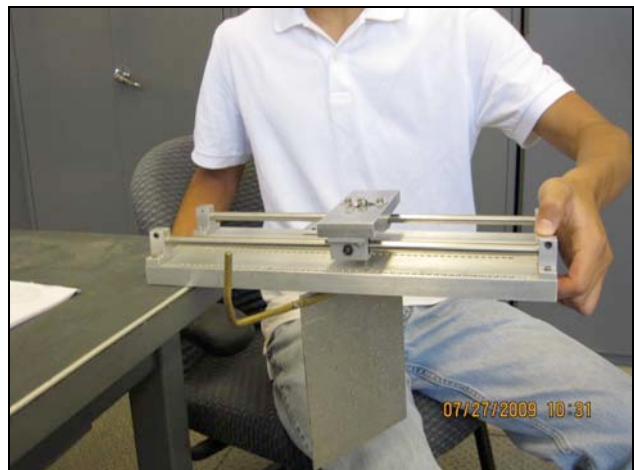


Fig. 4. Aerodynamically controlled power generator (wing at end-stroke).

Fig. 4 shows the model which we built in order to confirm the operating principle outlined

in the previous paragraph. The vertical foil is sliding on two rail guides. Also shown is the “finger”, but the two control rods are omitted in this photo.

Tests in two water tunnels and a towing tank showed that the foil started to oscillate quite satisfactorily for pitch axis locations between 60 to 70 percent of chord and water flow speeds exceeding 0.3 m/s. Two different foils were tested, a short aluminum foil of 14.3 cm chord and 18.6 cm span and a long foil of 14.3 cm chord and 30.5 cm span. The tests comprised the investigation of the effect of pitch axis location, maximum pitch angle setting and flow speed on the operation of the power generator. The flow speeds in the water tunnels ranged from 0.2 to 0.5 m/s and in the towing tank up to 1 m/s. Flow visualization photos and videos of the oscillator operation were taken to document the results. These tests, carried out in the Hydrodynamics Laboratory of the Naval Postgraduate School, are documented in a Master’s thesis by LT C. Semler and are currently being prepared for publication.

3 Numerical Simulations

3.1 Numerical Methodology

A number of simulations were performed to establish the effectiveness of flapping foil power generation. These involved single and tandem foil configurations undergoing both sinusoidal and non-sinusoidal prescribed motions, as well as a single foil undergoing fully flow-driven motion.

The unsteady flow field was simulated using the commercially available CFD package Fluent version 6.3.26, with an unsteady incompressible solver and second-order upwind spatial discretization.

Single foil calculations were performed using a moving inner mesh zone around the foil, and a fixed outer zone with a sliding interface between them. Pitching motion was achieved by rotating the inner zone, and plunging motion was achieved by incorporating a source term into the momentum equations in both zones and solving in a reference frame that moves with the foil. This method allows second-order accurate

time stepping, as detailed by Kinsey and Dumas [5].

Tandem foil configurations lack a single reference frame so the source term method cannot be used. Instead, the combined pitch and plunge motion was applied to a zone around each foil, and the intervening mesh was deformed and remeshed at each time step to maintain mesh quality using Fluent’s dynamic meshing feature. This limited time integration to first-order accuracy.

Power extraction was measured as the time-average of the contributions of the aerodynamic lift and moment:

$$P = \frac{1}{T} \int_t^{t+T} (L\dot{y} + M\dot{\theta}) dt \quad (1)$$

The efficiency was determined via comparison with the available power:

$$P_a = 0.5\rho U_\infty^3 y_{tot} \quad (2)$$

$$\eta = P / P_a \quad (3)$$

with y_{tot} = the total trailing edge excursion.

3.2 Verification and Validation

Details of mesh and timestep refinement studies for the source term and dynamic meshing methods, as well as validation against experimental results and other simulations, may be found in Ashraf et al [4].

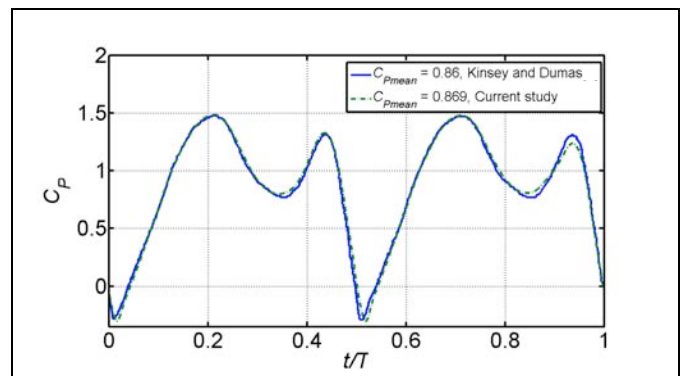


Fig. 5. Comparison of power coefficient time history, current work and Kinsey and Dumas[5].

Fig. 5 shows the good agreement in power coefficient time history between the current work and that of Kinsey and Dumas [5], for a NACA0015 foil pitching about 1/3 chord at reduced frequency $k = 2\pi fc / U_\infty = 0.88$, plunge

amplitude $h = 1.0$ chords, pitch amplitude $\theta_o = 76.3^\circ$, phase between pitch and plunge $\phi = 90^\circ$ (pitch leading plunge) and Reynolds number $Re = 1100$.

3.3 Single Foil Sinusoidal Motion

A NACA0014 foil pitching about $1/2$ chord at $Re = 20,000$, $k = 0.8$, plunge amplitude $h = 1.05$, and pitch amplitude $\theta_o = 73^\circ$ was simulated, using prescribed sinusoidal plunging and pitching motions. The physical geometry was chosen to be consistent with the experimental power generator. The flapping parameters were chosen with reference to Kinsey and Dumas [5] who simulated a NACA0015 foil pitching about $1/3$ chord at $Re = 1100$, $h = 1.0$, $\phi = 90^\circ$. In the range of frequency $k = 0.75 - 1.1$ and pitch amplitude $\theta_o = 70^\circ - 80^\circ$, they found efficiency up to 34%, comparable with high performance conventional wind turbines.

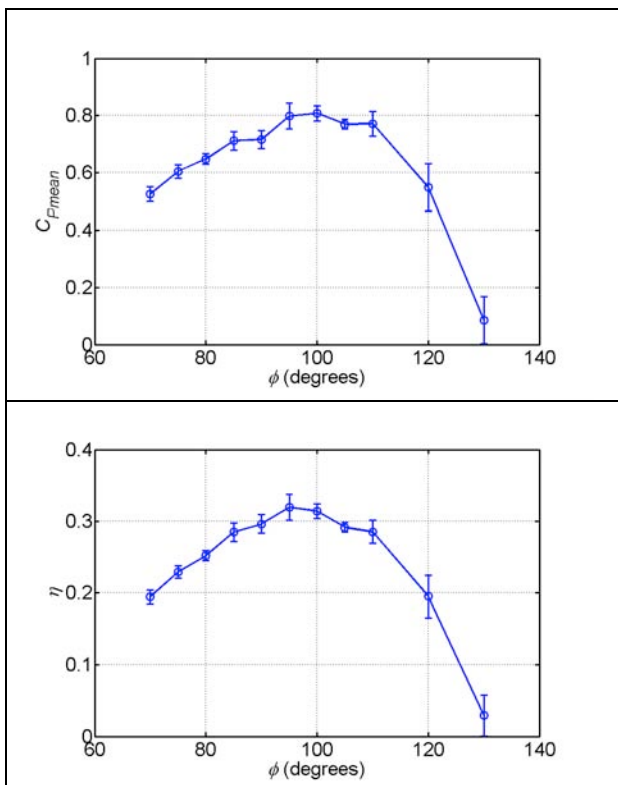


Fig. 6. Mean power coefficient and efficiency versus pitch-plunge phase angle.

The phase angle ϕ between pitch and plunge was varied between 70° and 130° (positive indicating pitch leading plunge). Fig. 6

shows that a relatively broad power coefficient and efficiency peak is found over a phase angle range from 90° to 110° , with an optimum at approximately 95° . At $Re = 20000$, the results show some variability in power coefficient from cycle to cycle. To account for this variability, each simulation was run for 15 flapping cycles and the mean of the last 12 flapping cycles is presented with error bars representing the standard deviation.

For $\phi = 70^\circ$ and 130° where the efficiency drops off significantly, large positive power is generated in the upstroke and downstroke, but this is counterbalanced by large negative power during the period of high rotation rate. In contrast $\phi = 90^\circ$ and 110° show only very small negative power peaks during foil rotation, and positive power is maintained for longer in the upstroke and downstroke. Further details may be found in Platzer et al [3].

3.4 Single Foil Non-Sinusoidal Motion

Kinsey and Dumas [5] noted that for the sinusoidal cases studied where high power coefficients were generated, the contribution to power is significantly dominated by the plunging motion compared with the pitching motion. Their findings as well as the results of the previous section suggest that an alternative foil motion may be preferable, where the foil plunge is maintained for as long as possible at a high velocity, followed by rapid pitching reversals. The aerodynamically controlled generator oscillates non-sinusoidally in just such a manner.

The motion of the generator is approximated in Fig. 7, with a period of constant translational velocity combined with a constant pitch angle, followed by a sinusoidal reversal of direction and pitch angle. The motion was characterized by the reversal time, ΔT_R , as a fraction of the total period (0.1 for rapid reversal, to 0.5 for fully sinusoidal motion). The pitching motion is shown leading the plunge by phase $\phi = 90^\circ$, for other phases the pitching motion was shifted left or right appropriately.

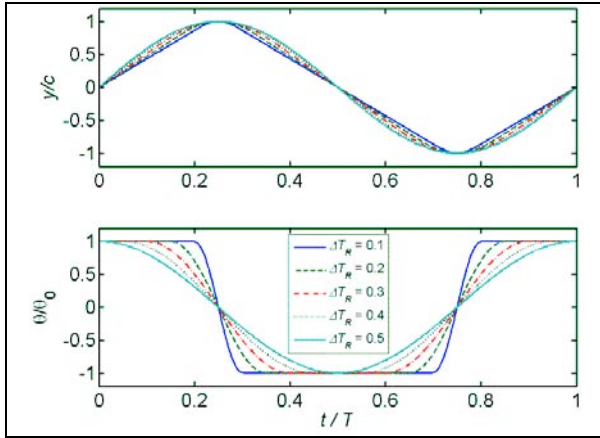


Fig. 7. Non-sinusoidal motions as a function of the stroke reversal time ΔT_R .

For comparison of the aerodynamically inspired motion with the usual sinusoidal motion, four phases based on the results in Fig. 4 were selected; $\phi = 70^\circ$ and 130° where the sinusoidal power and efficiency are low, and $\phi = 90^\circ$ and 110° at the locations where the power and efficiency are close to peak values. For these cases reversal times in the range $\Delta T_R = 0.1 - 0.5$ were considered. All other flapping parameters were kept the same, namely $k = 0.8$, $h = 1.05$, $\theta_o = 73^\circ$. The results shown in Fig. 8 indicate that $\Delta T_R = 0.3$ and $\phi = 90^\circ$ produce higher power and greater efficiency than for any of the sinusoidal motions considered.

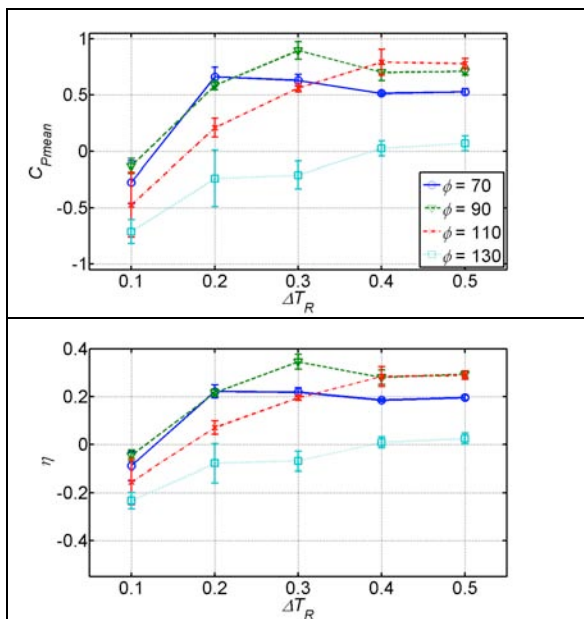


Fig. 8. Mean power coefficient and efficiency versus stroke reversal time, non-sinusoidal motions, $k = 0.8$, $h = 1.05$, $\theta_o = 73^\circ$.

Power generation in the non-sinusoidal cases is heavily influenced by the rotation rate, as determined by the stroke reversal time. For small ΔT_R (rapid rotation during stroke reversal), there is a large power input (negative power) required to initiate the foil rotation, followed by a positive power output once the rotation has been established. This rotational power input decreases, and the translational power output during the downstroke and upstroke becomes more uniform as ΔT_R increases. Further details may be found in Platzer et al [3].

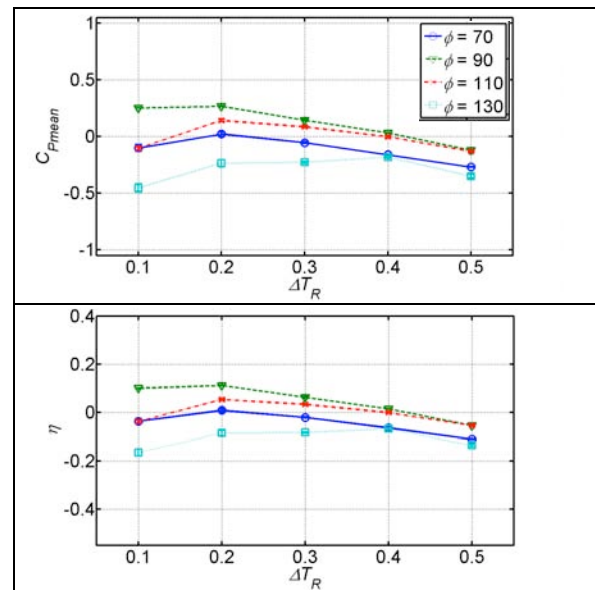


Fig. 9. Mean power coefficient and efficiency versus stroke reversal time, non-sinusoidal motions, $k = 0.8$, $h = 1.05$, $\theta_o = 40^\circ$.

In order to check whether these optimal values of ϕ and ΔT_R are dependent on plunge and pitch amplitudes, similar simulations were run for lower values of plunge and pitch amplitudes $h = 0.5$ and $\theta_o = 40^\circ$. Both power coefficient and efficiency are less sensitive to the phase ϕ especially for $\Delta T_R > 0.2$. Further, the results for low values of pitching amplitude $\theta_o = 40^\circ$ in Fig. 9 show quite different behavior than those for $\theta_o = 73^\circ$. For $\theta_o = 40^\circ$, only $\phi = 90^\circ$ $\Delta T_R = 0.1 - 0.4$ and $\phi = 110^\circ$ $\Delta T_R = 0.2 - 0.3$ provide positive power outputs, which are still very low compared to the $\theta_o = 73^\circ$ cases. This is also in accordance with the previous study of Kinsey and Dumas [5] and shows the

advantage of using larger pitch amplitudes for power generation.

The influence of flapping frequency was examined for the best case in Fig. 8, namely $\Delta T_R = 0.3$, $\phi = 90^\circ$, $h = 1.05$, $\theta_o = 73^\circ$, as shown in Fig. 10.

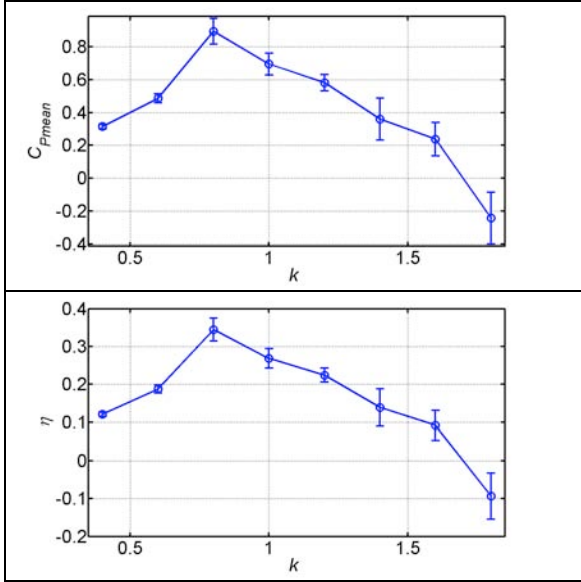


Fig. 10. Mean power coefficient and efficiency versus flapping frequency, time, non-sinusoidal motions, $\Delta T_R = 0.3$, $\phi = 90^\circ$, $h = 1.05$, $\theta_o = 73^\circ$.

The results in Fig. 9 show a peak in power coefficient and efficiency in the frequency range $k = 0.7 - 1.0$. At frequencies below this range, the plunging velocity remains very low, while for frequencies above this range the effective angle of attack is reduced significantly which causes reduction in lift and power.

3.5 Tandem Foils

The power generation obtained from close coupling of two flapping foils in tandem was examined as suggested by Jones et al [2]. As for the single foil cases, a NACA0014 foil pitching about 1/2 chord at $Re = 20000$, $k = 0.8$, $h = 1.05$, $\theta_o = 73^\circ$ was used. Sinusoidal (with $\phi = 90^\circ$) and non-sinusoidal (with $\phi = 110^\circ$) motions for both foils were prescribed, and the effect of the phase angle ψ between the leading and the trailing foils and the distance between the two pivot points X_{shift} was assessed.

The efficiency of power extraction for tandem foils is here defined as the ratio of the sum of power extracted by two foils divided by

the power available for the two foils (thus using twice the swept area). Results for the sinusoidal motions are shown in Fig. 11, and non-sinusoidal with $\Delta T_R = 0.3$ in Fig. 12.

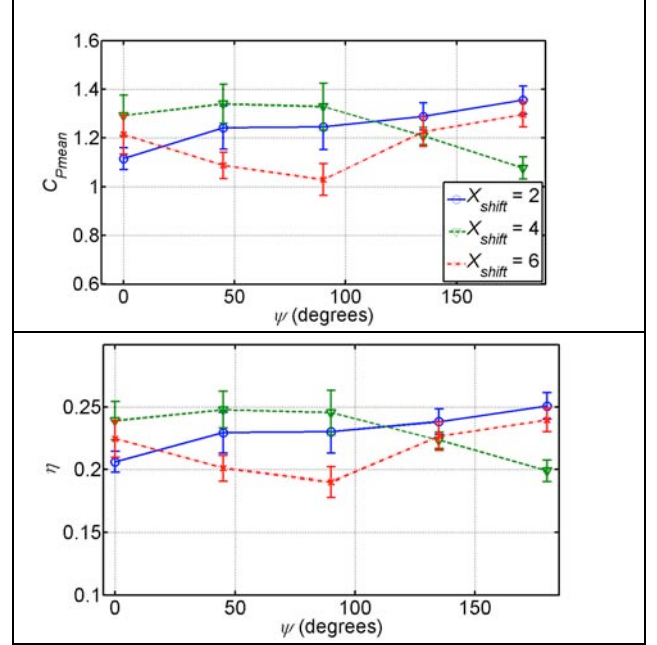


Fig. 11. Effect of phase angle between leading and trailing tandem foils, for various inter-foil distances, sinusoidal motion.

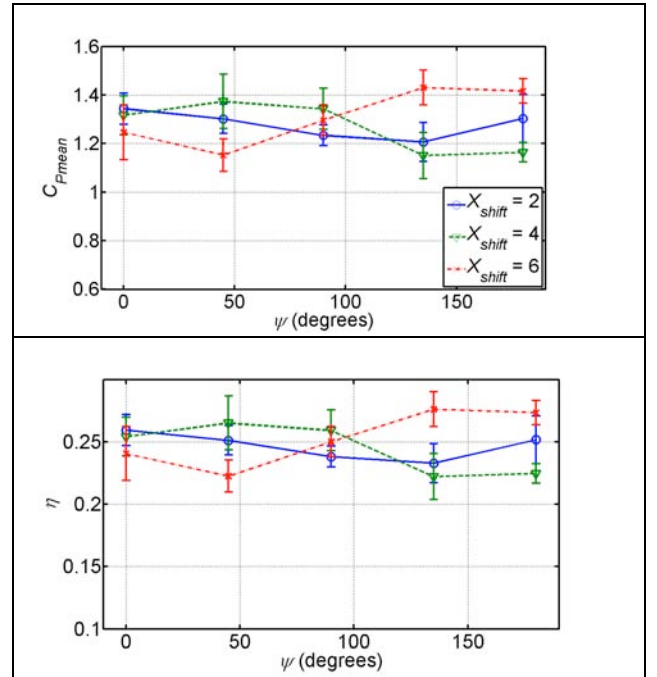


Fig. 12. Effect of phase angle between leading and trailing tandem foils, for various inter-foil distances, non-sinusoidal motion, $\Delta T_R = 0.3$.

Details of the time histories and flow fields for these cases may be found in Platzer et al [3]. Power and efficiency results are sensitive to both ψ and X_{shift} , indicating that the system may need to be tuned to achieve optimal placement of the trailing foil in the vortex wake of the leading foil, particularly as the flow speed varies.

Configuration	C_{Pmean} leading foil	C_{Pmean} trailing foil	Total C_{Pmean}	η
Single foil sinusoidal, ($\phi = 95^\circ$)	-	-	0.84 ± 0.04	0.32 ± 0.02
Single foil non-sinusoidal ($\Delta T_R = 0.3, \phi = 90^\circ$)	-	-	0.89 ± 0.07	0.34 ± 0.03
Sinusoidal tandem ($\phi = 110^\circ, X_{shift} = 2$ and $\psi = 180^\circ$)	0.80 ± 0.05	0.56 ± 0.01	1.35 ± 0.06	0.25 ± 0.02
Non-sinusoidal tandem ($\Delta T_R = 0.3, \phi = 90^\circ, X_{shift} = 6$ and $\psi = 135^\circ$)	1.00 ± 0.04	0.43 ± 0.05	1.43 ± 0.1	0.27 ± 0.05

Table 1. Comparison of performance of prescribed motion cases.

Table 1 shows a comparison of the maximum power coefficient output and efficiency for the best of each configuration assessed. It is evident that for a single foil generator, non-sinusoidal motions generate more power more efficiently than the sinusoidally driven generator. Further, using two foils in tandem either sinusoidally or non-sinusoidally appears to be more attractive in terms of power output of the system as a whole rather than the efficiency when compared with a single foil generator.

3.6 Single Foil Fully Flow Driven Motion

Much of the analysis and experiment in flapping wing power generation has focused on fully prescribed motions, as in the previous sections, or with one mode (e.g. pitch) prescribed and one (e.g. plunge) flow-driven (Zhu et al [6-7]).

Fully flow driven generators can be designed much more simply than mechanically driven turbines, as demonstrated in this paper. Analysis of prescribed motions gives an indication of which parameter combinations and motions may lead to high power outputs and efficiency, but does not address whether those motions can be achieved in practice. In particular, the frequency at which a flow-driven

foil will oscillate is a function of the oncoming flow speed, the mass and inertia of the foil and supporting mechanism, and the pitch and plunge amplitudes.

Further thought must be given to the manner in which power is extracted, as measuring only the power generated by the aerodynamic forces and moments on the foil (as done in the prescribed motion cases) results in a no-load situation. Accordingly the load on the foil from the power extraction mechanism must be built into the simulation. The load will also affect the frequency of oscillation that is achieved.

The fully flow driven turbine is simulated as shown in Fig. 13. Power is extracted from the plunge motion via a viscous damper. No power is extracted from the pitching component, as it simplifies the analysis and is in accord with the prescribed motion analysis indicating that the majority of power is available from the plunge mode.

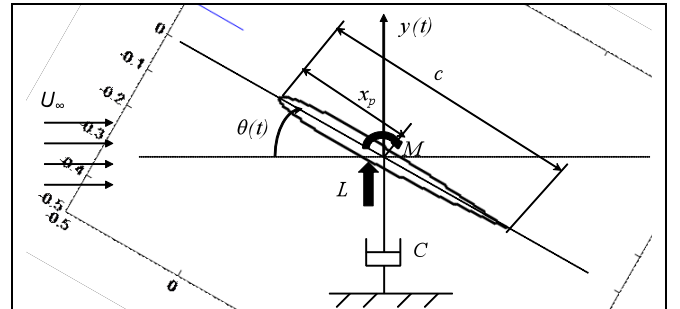


Fig. 13. Foil undergoing flapping motion in response to aerodynamic lift and moment

The conservation of energy equation for this system can be written as follows:

$$(L - C\dot{y})\dot{y} + M\dot{\theta} = m\dot{y}\ddot{y} + I\dot{\theta}\ddot{\theta} \quad (4)$$

where L is the aerodynamic lift, M is the aerodynamic moment, m is mass of the foil, I is the moment of inertia about the pivot point and C is the viscous damper strength.

In order to implement the fully flow driven flapping motion, both pitch and plunge positions are considered as a function of a mechanism angle β such that:

$$y = f(\beta) \quad (5)$$

$$\theta = g(\beta) \quad (6)$$

This allows any arbitrary combination of pitch and plunge motions, and phases between them, to be considered. Note that this reduces the system to a single degree of freedom, but still enables motions similar to that shown in the experiment to be simulated.

The equation of motion of the wing is solved in terms of the mechanism angle:

$$(mf_{\beta}^2 + Ig_{\beta}^2)\ddot{\beta} = \quad (7)$$

$$Lf_{\beta} + Mg_{\beta} - Cf_{\beta}^2\dot{\beta} - (mf_{\beta}f_{\beta\beta} + Ig_{\beta}g_{\beta\beta})\dot{\beta}^2$$

Eqn (7) is solved within Fluent using sub-iteration at each physical time step. Lift and moment values are calculated at the start of each sub-iteration. Then the mechanism angle β is calculated in response to aerodynamic lift and moment, pitch and plunge motions determined, the foil is moved and lift and moment recalculated until convergence is achieved. The mechanism angle approach has the significant advantage that it avoids large numerical spikes in linear and rotational accelerations (and hence aerodynamic forces) when the foil strikes a pitch or plunge limit.

In order to directly compare with the prescribed motion case of Kinsey and Dumas [5] (NACA0015, $h = 1.0$, $\theta_o = 76.3^\circ$, pitching about $1/3$ chord from the leading edge, $\phi = 90^\circ$), the fully flow driven motion case is simulated at the same parameters with flow $Re = 1100$.

The external load is defined in the form of non-dimensionalized damping coefficient, $C' = C/\pi\rho_{air}cU_{\infty}$, where, C is the damping coefficient and $\pi\rho_{air}cU_{\infty}$ is the equivalent damping due to the added mass effect as employed by Zhu et al [6]. The power output is defined as

$$P = C \dot{y}^2 \quad (8)$$

Available power and efficiency are determined as for the prescribed motion cases. The mass and inertia of the foil were based on the experimental setup described in Section 2, but with an equivalent unit span (foil mass $m = 5.75$ kg, moment of inertia $I = 0.479$ kg m²).

The mesh used for the fully flow driven simulations is the same as for the prescribed motion cases, with a rotating inner mesh zone

and the source term method is again used to introduce the plunge motion.

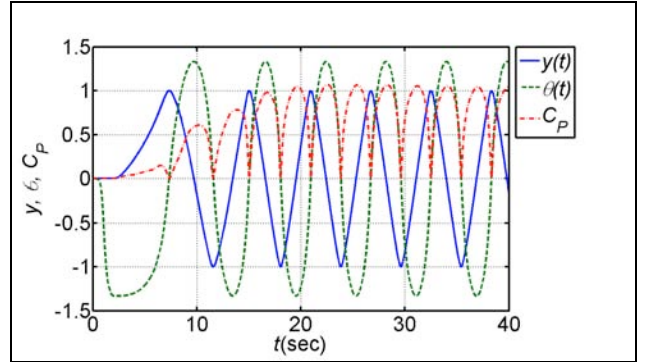


Fig. 14. Fully flow driven motion, damper ratio $C' = 0.25$.

Plunge motion y and pitch angle θ are here given as sinusoidal functions of mechanism angle β , however this does not necessarily result in sinusoidal motions in time (which would only be true if β were to increase uniformly in time). This may be seen in Fig. 14 which shows time histories of y , θ and C_P for $C' = 0.25$. The plunge motion in this case is close to a triangular wave in time. The smooth operation of the fully flow driven power generator can be seen in this plot, and the frequency and amplitudes become uniform in time after the 3rd cycle of oscillation.

Configuration	k	C_{Pmean}	η
Prescribed motion	0.88	0.86	0.33
$C' = 0.125$	1.26	0.55	0.21
$C' = 0.25$	1.06	0.77	0.30
$C' = 0.375$	0.66	0.45	0.17
$C' = 0.5$	0.43	0.27	0.11
$C' = 1.0$	0.28	0.23	0.10

Table 2. Fully flow driven results for different damper ratios.

Table 2 shows a comparison of prescribed motion generator results and fully flow driven power generator at different damping. The fully flow driven generator produces comparable power and efficiency to the prescribed motion at damper ratio $C' = 0.25$. The frequency, power output and efficiency are all sensitive to the damper ratio, with the power and efficiency showing peaks that indicates an optimum damping strength that is likely to vary with the

mass and inertia of the foil, the flow speed, the plunge and pitch amplitudes and the kinematics.

For the tested parameters, the maximum power output and efficiency in the fully flow driven case is achieved relatively close to the reduced frequency predicted by the prescribed motion analysis, which suggests that the conclusions of that analysis are still valid.

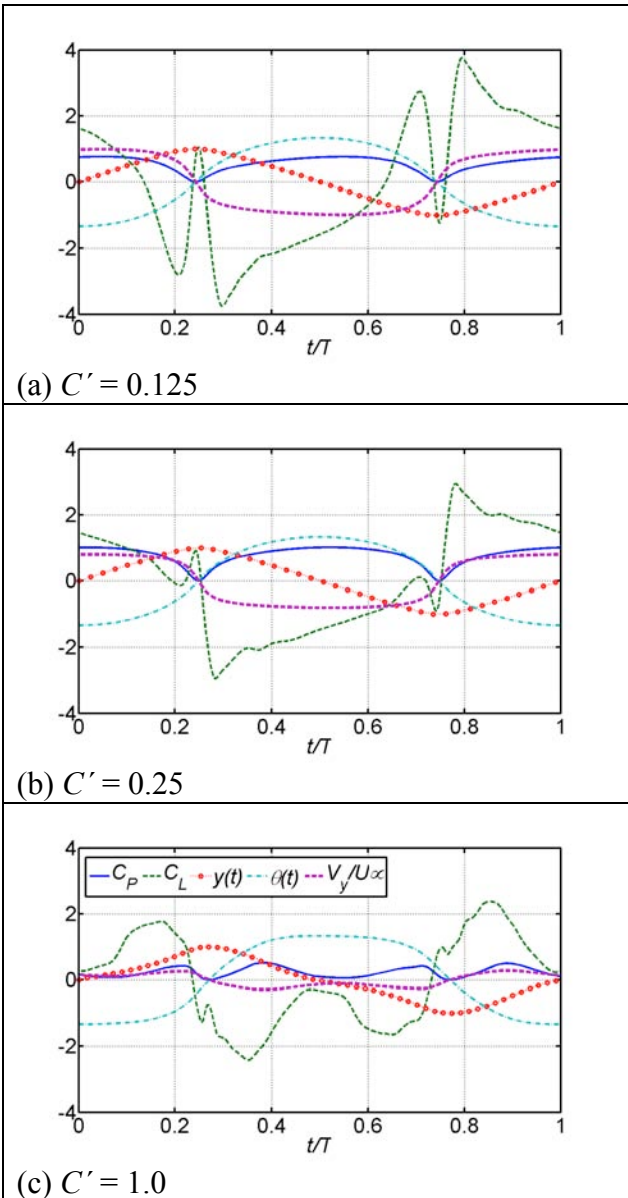


Fig. 15. Instantaneous power coefficient, lift coefficient, foil motion and velocity for fully flow driven cases.

The instantaneous power coefficient, lift coefficient, y position, θ and y velocity are shown in Fig. 15 for several different damping coefficients (all values plotted on the same

vertical scale). The non-sinusoidal motion actually achieved is apparent in this figure.

For $C' = 0.25$, C_L and V_y are well synchronized and also the V_y is comparatively higher than for $C' = 1.0$, which causes the increased power output. For $C' = 0.125$, V_y is even higher than for $C' = 0.25$ but the synchronization between lift and velocity is poor which results in loss of power (see Fig. 15a, $t/T = 0.25$ and 0.75 for $C' = 0.125$). For higher damping coefficients ($C' > 0.25$), although the C_L and plunge velocity have same signs for most part of the flapping cycle, the magnitude of the plunge velocity is quite low which reduces the power output.

Fig. 16 shows the upper and lower surface pressure coefficient distributions and the pressure fields at $t/T = 0.2$ for $C' = 0.125$, $C' = 0.25$ and $C' = 1.0$.

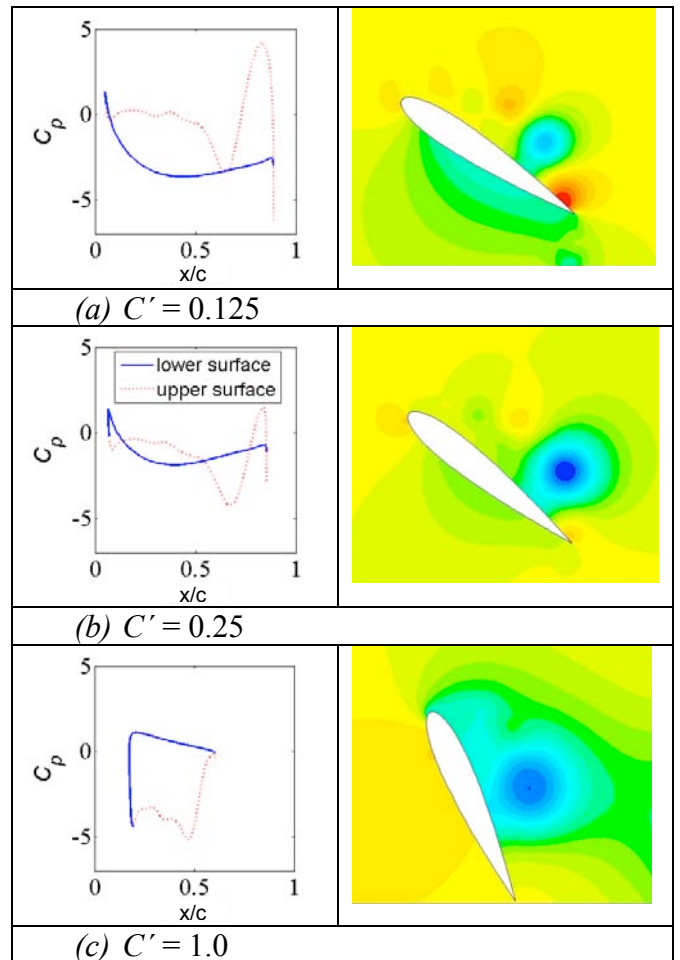


Fig. 16. Surface and field pressure coefficient at $t/T = 0.2$ for three different damper ratios.

At this instant, the foil is moving upward but due to the different frequencies, the surface pressure and hence the aerodynamic forces are different in each case. For $C' = 0.125$, the surface pressure distribution shows large lift in the direction opposing the motion (due to the difference in surface pressure on lower and upper surface of the foil caused by massive separation at the leading edge; very high pressure near the trailing edge and relatively lower pressure on the lower surface of the foil). For $C' = 0.25$, the surface pressure distribution for upper and lower surfaces almost cancel each other out and cause a small lift in the direction opposing the vertical motion so that there is minimal loss of power during rotation of the foil. For $C' = 1.0$, large lift (due to the massive flow separation over the upper surface of the foil) is being generated in the direction of motion but the magnitude of the velocity is quite low. Also the pitch amplitude is still very high at this instant so the aerodynamic lift opposes the rotation and a large amount of power is lost in rotating the foil at this damping coefficient.

4 Conclusions

It has been shown that a fully flow driven flapping wing power generator is practical without the need of an external motor to induce one mode of motion. However much work remains to determine optimum power generation parameters, as the results presented here are only limited to particular values of pitch and plunge amplitudes, pivot point location, mass of the foil and incoming flow speed.

5 Contact Author Email Address

platzer@redshift.com

Copyright Statement

The authors confirm that they, and/or their company or organization, hold copyright on all of the original material included in this paper. The authors also confirm that they have obtained permission, from the copyright holder of any third party material included in this paper, to publish it as part of their paper. The authors confirm that they give permission, or have obtained permission from the copyright holder of this paper, for the publication and

distribution of this paper as part of the ICAS2010 proceedings or as individual off-prints from the proceedings.

References

- [1] Platzer, M.F., Young, J., and LAI, J.C.S. (2008). "Flapping-Wing Technology: The Potential for Air Vehicle Propulsion and Airborne Power Generation", *26th Congress of the International Council of the Aeronautical Sciences (ICAS)*, Anchorage, Alaska, 14-19 Sep 2008.
- [2] Jones, K.D., Lindsey, K., and Platzer, M.F. (2003). "An Investigation of the Fluid-Structure Interaction in an Oscillating-Wing Micro-Hydropower Generator", *Fluid-Structure Interaction II, Wessex Institute of Technology Press*, pp. 73-82.
- [3] Platzer, M.F., Ashraf, M.A., Young, J., and Lai, J.C.S. (2009). "Development of a New Oscillating-Wing Wind and Hydropower Generator", *47th AIAA Aerospace Sciences Meeting*, Orlando, Florida, 5-8 Jan 2009.
- [4] Ashraf, M.A., Isaacs, A., Young, J., Lai, J.C.S., and Ray, T. (2009). "Numerical Simulation And Multi-Objective Design Of Flow Over Oscillating Airfoil For Power Extraction", *Conference on Modelling Fluid Flow (CMFF'09), 14th International Conference on Fluid Flow Technologies*, Budapest, Hungary, September 9-12, 2009.
- [5] Kinsey, T., and Dumas, G. (2008). "Parametric Study of an Oscillating Airfoil in a Power-Extraction Regime," *AIAA Journal* Vol. 46, No. 6, pp. 1318-1330, doi: 10.2514/1.26253.
- [6] Zhu, Q., Haase, M., and Wu, C.H. (2009). "Modeling the capacity of a novel flow-energy harvester," *Applied Mathematical Modelling* Vol. 33, pp. 2207-2217.
- [7] Zhu, Q., and Peng, Z. (2009). "Mode coupling and flow energy harvesting by a flapping foil," *Physics of Fluids* Vol. 21, No. 3, pp. 033601-1 to 10.